ARMY RESEARCH LABORATORY

Nondestructive Characterization of Low Velocity Impact Damage in Transparent Laminate Systems

by Raymond E. Brennan and William H. Green

ARL-TR-5582 **June 2011**

NOTICES

Disclaimers

The findings in this report are not to be construed as an official Department of the Army position unless so designated by other authorized documents.

Citation of manufacturer's or trade names does not constitute an official endorsement or approval of the use thereof.

Destroy this report when it is no longer needed. Do not return it to the originator.

Army Research Laboratory
Aberdeen Proving Ground, MD 21005-5066

ARL-TR-5582 **June 2011**

Nondestructive Characterization of Low Velocity Impact Damage in Transparent Laminate Systems

Raymond E. Brennan and William H. Green
Weapons and Materials Research Directorate, ARL

REPORT DOCUMENTATION PAGE

Form Approved
OMB No. 0704-0188

1. REPORT DATE *(DD-MM-YYYY)*	2. REPORT TYPE	3. DATES COVERED (From - To)
June 2011	Final	April 2010 to April 2011

4. TITLE AND SUBTITLE
Nondestructive Characterization of Low Velocity Impact Damage in Transparent Laminate Systems

5a. CONTRACT NUMBER

5b. GRANT NUMBER

5c. PROGRAM ELEMENT NUMBER

6. AUTHOR(S)
Raymond E. Brennan and William H. Green

5d. PROJECT NUMBER

5e. TASK NUMBER

5f. WORK UNIT NUMBER

7. PERFORMING ORGANIZATION NAME(S) AND ADDRESS(ES)
U.S. Army Research Laboratory
ATTN: RDRL-WMM-E
Aberdeen Proving Ground, MD 21005-5066

8. PERFORMING ORGANIZATION REPORT NUMBER
ARL-TR-5582

9. SPONSORING/MONITORING AGENCY NAME(S) AND ADDRESS(ES)

10. SPONSOR/MONITOR'S ACRONYM(S)

11. SPONSOR/MONITOR'S REPORT NUMBER(S)

12. DISTRIBUTION/AVAILABILITY STATEMENT
Approved for public release; distribution unlimited.

13. SUPPLEMENTARY NOTES

14. ABSTRACT
Advanced transparent materials are used to improve protection efficiency for lightweight vehicles and Warfighters in applications such as face shields, riot gear, and vehicle windows. If any damage occurs, the ability to withstand single or multiple hits from various threats could be compromised. While these issues are most likely to occur due to impacts from high velocity projectiles during combat, they may also be the result of low velocity impacts from collisions, severe environmental conditions, or foreign object debris. In this study, transparent materials are tested by comparing baseline conditions to experimentally controlled damage states. Destructive testing including air gun and sphere impact testing are used to simulate low velocity impacts in the field. Characterization of the damaged state includes visual inspection, cross-polarization, x-ray, and ultrasound techniques. The combination of destructive testing and characterization of the resulting damage can help to establish a damage acceptance criterion for transparent materials used in protective systems.

15. SUBJECT TERMS
Damage, characterization, transparent, ultrasound, NDE

16. SECURITY CLASSIFICATION OF:			17. LIMITATION OF ABSTRACT	18. NUMBER OF PAGES	19a. NAME OF RESPONSIBLE PERSON
a. REPORT	b. ABSTRACT	c. THIS PAGE			Raymond E. Brennan
Unclassified	Unclassified	Unclassified	UU	30	19b. TELEPHONE NUMBER (*Include area code*) (410) 306-0913

Contents

List of Figures

Acknowledgment

We would like to acknowledge Parimal Patel, Jian Yu, Terrence Taylor, and Dave Spagnuolo of the U.S. Army Research Laboratory for their efforts and support.

INTENTIONALLY LEFT BLANK.

1. Introduction

Individual transparent materials used in protective systems typically consist of glass, polymeric, and ceramic materials. These material components are often stacked and adhered by polymer interlayers to form transparent laminate protective systems (*1*). The presence of potentially harmful internal defects in these individual materials (pores, inclusions, secondary phases, etc.) and interlayer defects in the laminates (disbonds, delaminations, etc.) can reduce material properties but may not be visually detectable if index-matched.

Nondestructive bulk characterization techniques can be used in the pre-impacted state to detect material inhomogeneities and improve quality control for transparent materials before they are used in the field. They can also be used post-impact to detect resulting damage or compare baseline and damaged states for determination of critical impact conditions.

Current strike face glasses used in transparent laminate protective systems are limited in how thin they can be fabricated before encountering durability issues. Lower density novel glass compositions have been developed that can be fabricated more than 10 times thinner while maintaining their durability. By reducing the thickness and lowering the density of the strike face glass, the overall weight will also be reduced. Weight reduction is desirable for vehicle systems to increase maneuverability and transportability while reducing operational costs (*1*). This study focuses on a comparison of current and novel glasses used in transparent laminate systems and their ability to withstand low velocity impact damage. Success is measured qualitatively by how severe the damage impairs visibility and quantitatively by the damage measured through nondestructive imaging methods.

2. Experimental

The transparent materials chosen for this study were four 14-in by 14-in laminate panels. Identical 740-series glass laminate panels, denoted 740-1 and 740-2, each contained three glass and two adhesive layers. The thickness of each panel was ~16 mm. The layers consisted of a strike face layer (Borofloat® borosilicate glass [*2*]), an adhesive bonding layer, a second glass layer (Starphire® soda-lime-silicate glass [*3*]), a second adhesive bonding layer, and a polycarbonate backing layer. Two additional 741-series glass laminate panels were fabricated with four of the same five layers as the 740-series. In these panels, the strike face glass layer was changed to a thinner and lower density material (Eagle® glass [*4*]), making the total thickness ~11 mm. The 740 and 741-series panels were subject to the same low velocity impact conditions and compared to one another.

Air gun testing was used on 740-1 and 741-1 as a higher mass/lower velocity technique. This method used ~19-mm steel spheres to impact the panels. The average impact velocity for the air gun tests was ~30 m/s. In contrast, sphere impact testing was used on 740-2 and 741-2 as a lower mass/higher velocity technique. Impact testing was conducted using ~5-mm steel spheres. Each sphere was launched from a pneumatic launcher at velocities averaging ~400 m/s. For both techniques, a high-speed camera was set up 90^{o} to the projectile path to measure impact velocity.

Visual characterization was conducted on pre-impacted panels by observing visible defects and on post-impacted panels by identifying visible damage. Each panel was illuminated by white light from a light box and digital images were collected for documentation of the pre- and post-impacted states of each panel (figure 1). Cross-polarization techniques were used to observe residual stress states in the transparent laminate systems. The panels were placed between polarized films oriented 90^{o} to one another and illuminated by white light from a light box. When polarized light passed through each panel, the components of the light wave that were parallel and perpendicular to the direction of the stress propagated at different speeds (*5, 6*). This effect, referred to as retardation, was proportional to the degree of residual stress in the material. It was visibly displayed as a series of fringes that varied in color and intensity. The degree of stress in the transparent laminates was interpreted based on the color patterns by using the Michel-Levy birefringence chart (*7*). Digital cross-polarized images were collected for documentation of the pre- and post-impacted states of each panel (figure 1).

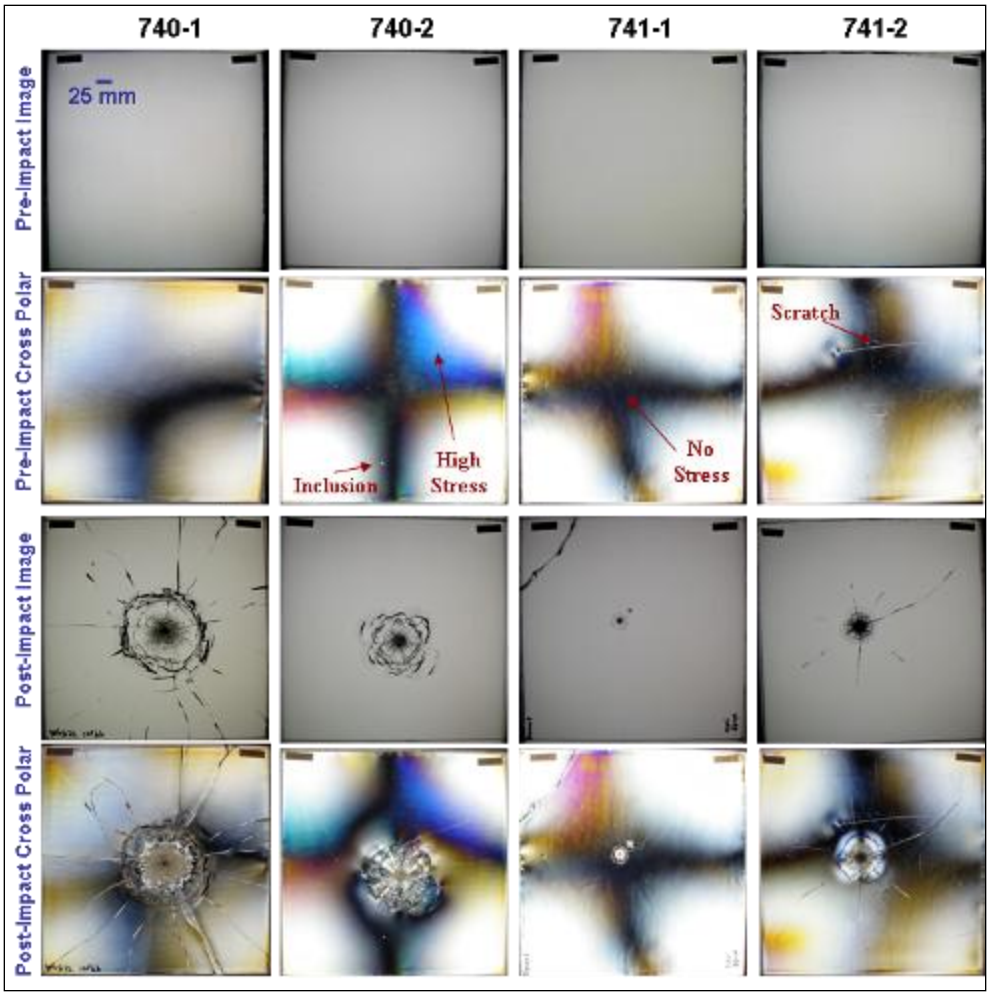

Figure 1. Visual characterization and cross-polarized digital images pre- and post-impact.

For radiographic inspection, a beam of penetrating radiation was passed through the transparent laminate systems in a non-invasive manner. While x-ray digital radiography (DR) was used as a two-dimensional (2-D) method to produce digital images of the full panels, x-ray computed tomography (XCT) provided densitometric images of thin cross sections through each panel (figure 2) (*8*, *9*). Projection DR and XCT were performed through the thickness of the transparent laminate panels using a computed tomography system with a 420-kVP x-ray source and a 512-element linear detector array. The tube energy and current used were 400 keV and 2.0 mA, respectively, and the focal spot was 0.80 mm. The source-to-image-distance and source-to-object-distance were 940.00 and 750.00 mm, respectively.

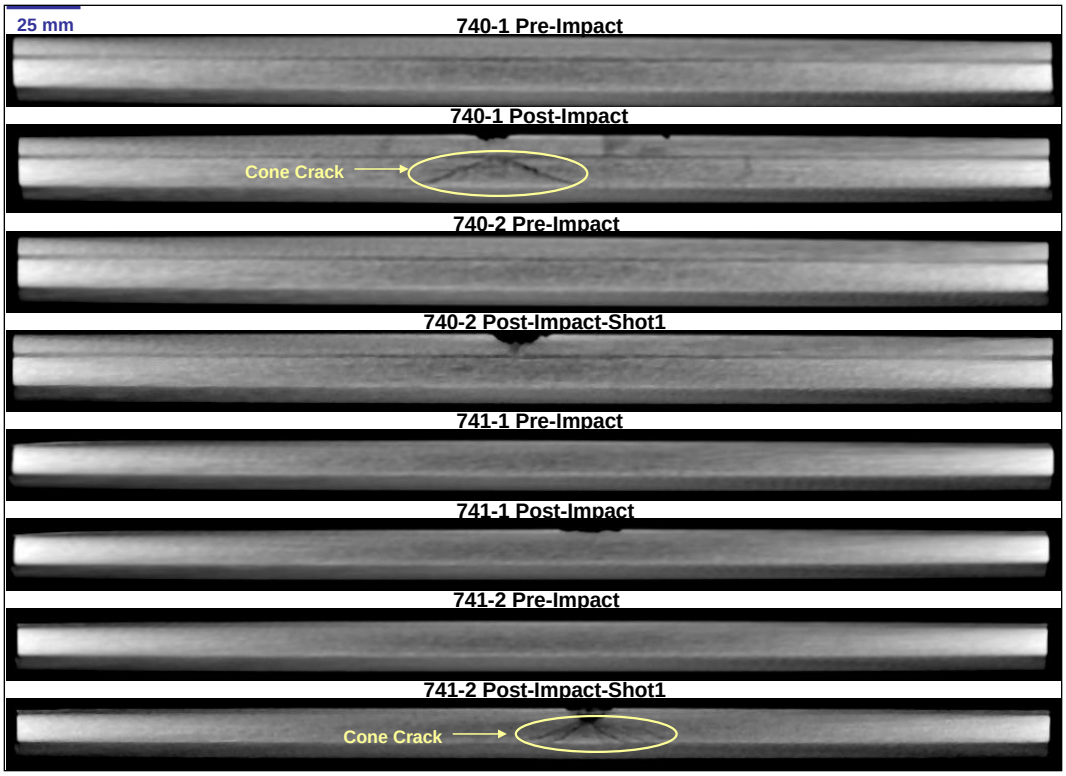

Figure 2. XCT cross-sectional images pre- and post-impact.

Ultrasound (UT) characterization was used to detect material variations, defects, and damage in the transparent laminate panels. As the acoustic waves were transmitted into the panels, material changes in individual glass or polymer layers (pores, inclusions, cracks) or laminate interlayers (disbonds, delaminations) resulted in acoustic impedance mismatches that caused reflection of the waves (*10*, *11*). The reflected acoustic waves were selected, gated, and collected as a function of signal amplitude, or intensity. Reflected signals from the top surface of the panels were used to collect surface/near-surface data while bottom surface reflected signals were used to collect bulk data through each panel. Spatial maps, or ultrasound C-scan images, of the gated signals were used to form visual plots of acoustic variations caused by defects and/or damage. Ultrasonic testing was conducted using a 64-element 10-MHz linear phased array transducer. A total of 32 active transducer elements were used for each scan, with active area dimensions of 32.0 mm length, 0.5 mm pitch, and 7.0 mm elevation. The transducer was mounted to a scanning bridge for motion control in the *x*-, *y*-, and *z*-axes during setup and testing. A water immersion tank was used to contain the panels during scanning.

3. Visual and Cross-polarization Characterization

Through visual characterization, several millimeter-sized inclusions were found in the transparent laminate panels, numbering ~14 in 740-1, ~18 in 740-2, ~11 in 741-1, and ~36 in 741-2. In 741-2, two surface scratches and cracking damage at the upper edge of the panel were also visible (figure 1). Through cross-polarization imaging, variations in stress patterns were observed (figure 1). According to the Michel-Levy birefringence chart, the black regions represented areas with no stress, the white regions represented areas with minimal stress, the yellow-orange regions represented areas with a significant degree of stress, and the red-blue regions represented areas with a relatively high degree of stress (*7*). Despite the panels being fabricated in the same manner, the stress patterns appeared to be drastically different. While 740-1 showed minimal stress with some yellow-orange regions near the edges, 740-2 showed large regions of high stress throughout the center. Panels 741-1 and 741-2 showed some significant yellow-orange stress regions, with 741-2 exhibiting a high stress region near two of the largest inclusions.

After impacting the series 1 panels with the air gun and the series 2 panels using sphere impact testing, the laminates were observed and compared to their pre-impacted states. The first qualitative observation from the digital images was that the degree of damage appeared to be greater for the thicker 740-series laminates. This was especially evident when comparing the impact damage diameter of ~168 mm and extensive radial cracking in 740-1 to the minimal impact damage diameter of ~28 mm and absence of radial cracking in 741-1. The crack in the upper left corner of 741-1 was believed to be caused by the clamp used to hold the panel in place during air gun testing. For the sphere impact tested panels, the ~132-mm-diameter damage at the impact region of 740-2 was approximately twice the size of the ~63-mm-diameter damage of 741-2. However, for the higher velocity sphere impact testing, the crack formation trend was reversed, with radial cracking present in the thinner laminate panel but not in the thicker laminate. When observing the impacted panels through cross-polarizers, some local stress variations were found, but the overall patterns did not appear to be drastically altered. There was an observable change in 740-2 that appeared to indicate stress relief after impact, in which a blue high stress region changed to a black region where no stress was apparent. In contrast, the impact region of 741-2 appeared to show concentric high stress regions in the same orientation of what was perceived to be a cone crack at the point of impact. Overall, the 740-series panels exhibited a higher degree of damage after impact when compared to the 741-series panels. As the velocity was increased and mass decreased from air gun to sphere impact testing, the magnitude of damage was reduced from 20 times larger (740-1 vs. 741-1) to twice as large (740-2 vs. 741-2). In terms of visibility through the transparent panels, the 741-series panels performed better, as the degree of damage was less pervasive.

4. Digital Radiography and X-ray Computed Tomography Characterization

The DRs of the pre-impacted panels were unable to detect any distinguishable features. All of the images appeared to be homogeneous, as the inclusions and surface scratches could not be resolved. On the other hand, the XCT images detected and contrasted the laminate layers effectively (figure 2). For the 740-series panels, the Borofloat strike face layer, Starphire interlayer, and polycarbonate backing layer were readily apparent in the cross-sectional image slices. Although the Eagle glass strike face layers in the 741-series panels were 12 times thinner than the Borofloat strike face layers, they could still be resolved in the XCT images, though this was more difficult near the edges.

After impact, the DRs showed damage at the immediate impact point where the sphere struck the panel, but the extent of damage in the surrounding area was unable to be resolved. For 740-1, the radial cracks were apparent upon careful observation, and appeared as hairline cracks extending from the central impact location to the edge of the panel. However, the radial cracks observed in the visual and cross-polarized images for 741-2 could not be resolved in these DRs. The XCT cross-sectional slices captured from the center of each impact were much more revealing (figure 2). For 740-1, inspection of the strike face showed the amount of material ejected after impact and indicated how deep the damage extended below the surface. The most interesting feature was the cone crack that formed at the top of the Starphire layer and extended all the way through this second layer. While it was difficult to distinguish damage at different layers through visual observation, the XCT images provided a definitive distinction of damage as a function of depth. In contrast to 740-1, the XCT image of 740-2 indicated that the damage at the impact site did not extend all the way through the strike face layer and that the second layer remained undamaged. For 741-1, the damage appeared to occur only in the Eagle glass strike face layer, while the damage in 741-2 extended into the Starphire layer and formed another cone crack similar to the one observed in 740-1. These results were consistent with the optical images, as panels that restricted the damage to the strike face layer did not result in radial cracking, while panels that allowed penetration into the second layer resulted in radial cracking and more extensive damage. While the DRs provided little information beyond impact location, XCT images provided a wealth of information for effective characterization through the depth of each panel.

5. Ultrasound C-scan Imaging Characterization

For the first set of pre-impact C-scan images, the surface/near-surface reflected signal was gated and the changes in the amplitude of the signal were mapped (figure 3). Each panel was scanned

through the strike face as well as the back face to observe acoustic variations from either side (figure 3). While the 740-series samples appeared to be relatively homogeneous, surface/near-surface inclusions were detected that were consistent with visual observations.

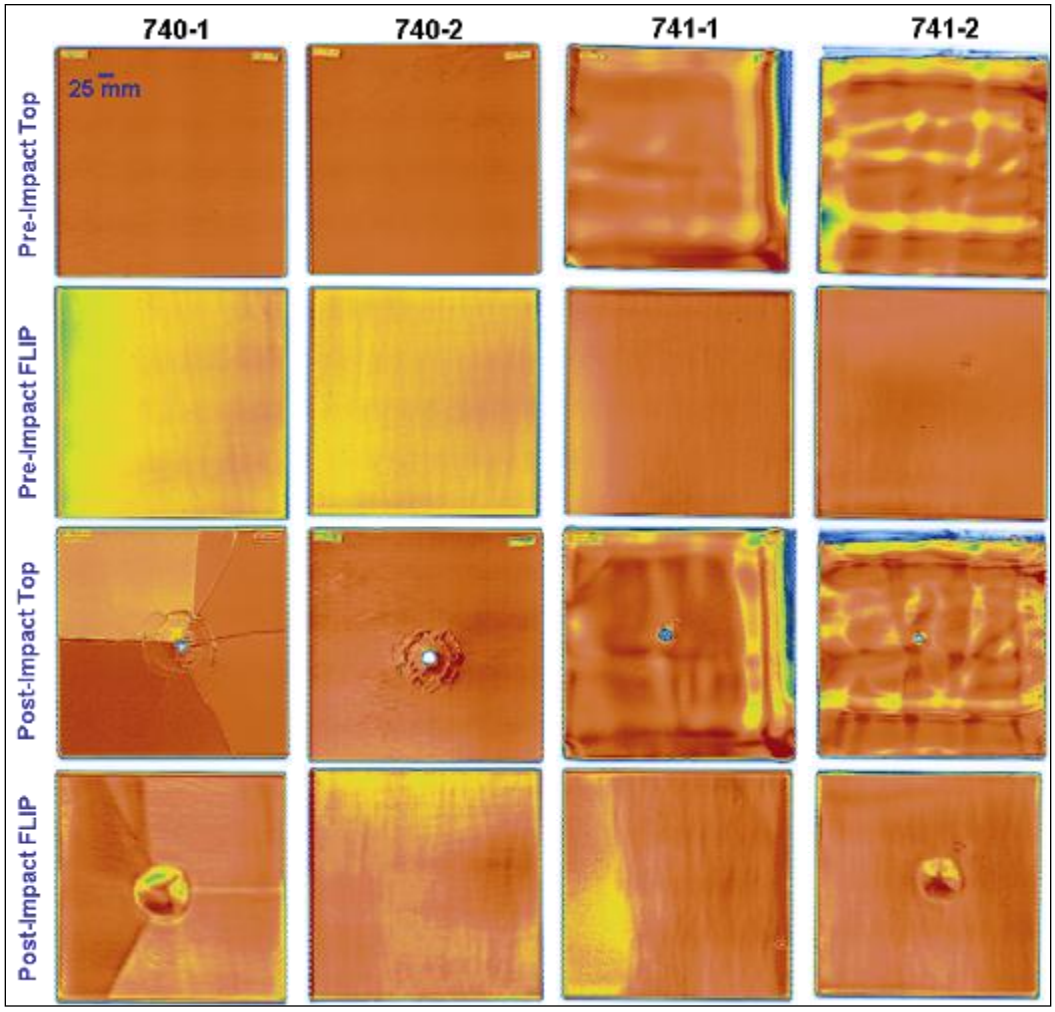

Figure 3. Surface/near-surface UT C-scan images pre- and post-impact.

An interesting phenomenon occurred upon observation of the 741-series. Due to the reduced thickness of the Eagle glass strike face layer, significant amplitude variations caused by surface variations and uneven deposition of adhesive layers in the near-surface were detected. Since the C-scan images collected through the strike face side of these panels were sensitive to adhesive variations, a much greater contrast was apparent. When these same panels were ultrasonically imaged through the back face, these features were not detected, and the results were comparable to those of the 740-series panels scanned in the same orientation. The damage to the upper edge of 741-2 was also distinguished in the C-scan images, as a lower amplitude signal was evident where pre-impact cracking was present.

For the second set of images, the bottom surface reflected signal was gated and the amplitude changes through the entire bulk of each panel were evaluated (figure 4). The 740-series panel scans were once again homogeneous. The only distinguishable features were inclusions with lower amplitude values than the rest of the panel. The 741-series panel scans showed more intricate adhesive patterns through the thinner strike face glass layers. In this case, the scans through the back face also showed adhesive patterns in which there were acoustic variations. A vertical band on the left side of 741-1 and parallel horizontal bands in the upper and lower regions of 741-2 were indicative of these patterns. As opposed to the previous scans that only showed surface/near-surface amplitude variations, the bottom surface scans represented a greater volume of the sample and enabled similar adhesive features to be observed through both sides of each panel.

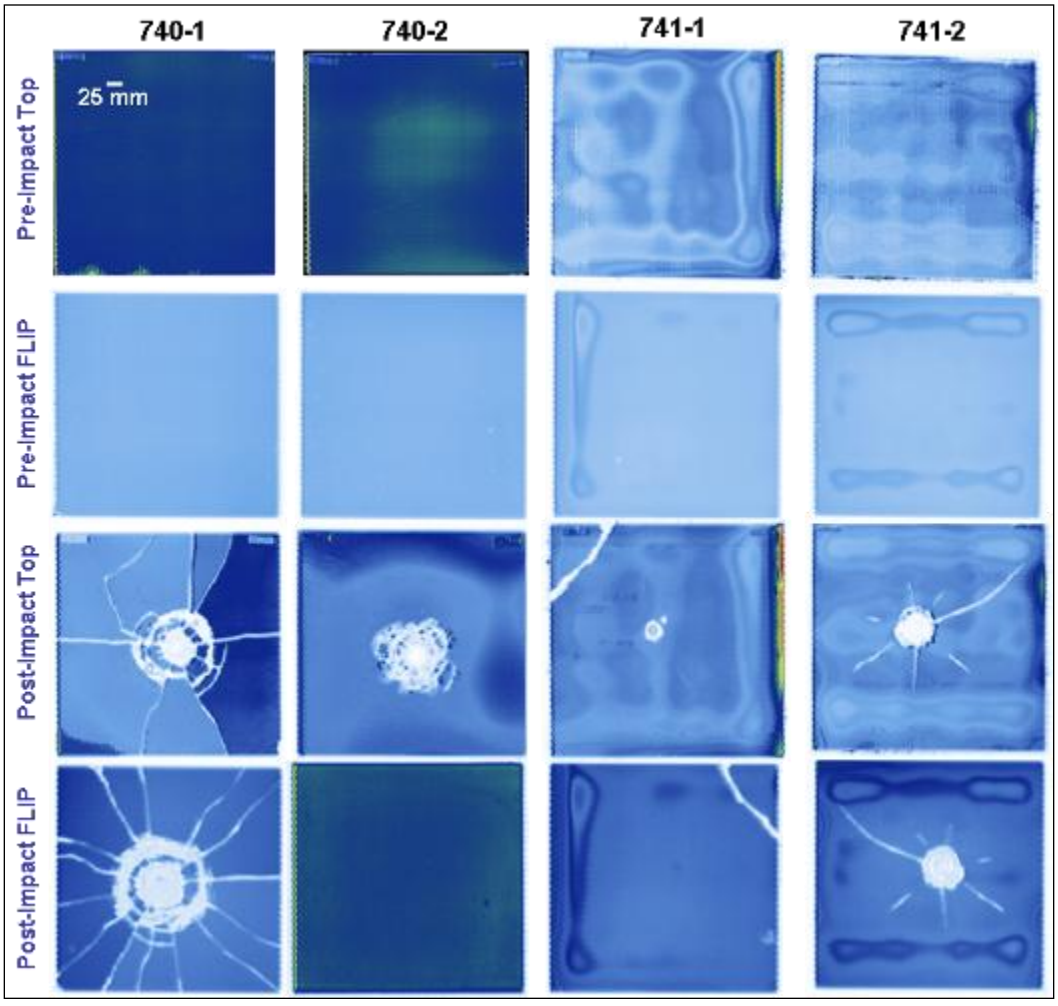

Figure 4. Bottom surface reflected signal UT C-scan images pre- and post-impact.

After impact, the ultrasound C-scan images were adept at showing the damage in great detail. For 740-1, the surface/near-surface scans showed the point of impact as a complete loss of amplitude (figure 3). The cone cracks as well as the radial cracks were also observed in these

images, in contrast to the DRs, which were only able to resolve the radial cracks. The C-scan images through the back face of 740-1 showed a circular region representative of the bulge that occurred in the polycarbonate backing layer post-impact. The dimensional change was an observation unique to the C-scan images and was found in both 740-1 and 741-2, the two samples in which damage to the Starphire layer was identified in the XCT images. For the other two samples, C-scan images through the back face revealed no isolated regions of damage. For the 741-series samples, the adhesive pattern variations appeared to change upon impact to the panels. This could have been an indication of physical change to the adhesive layers, which were designed to mitigate stress and prevent crack propagation into successive layers (*1*).

The bottom surface reflected signal C-scan images though the bulk of each sample were very effective at contrasting damage, with cracked or damaged regions resulting in a complete loss of signal (figure 4). For 740-1, scanning through the strike face showed crack patterns within the Borofloat layer, while scanning through the back face showed crack patterns in the Starphire layer. While several cracks were able to penetrate both layers, the majority of the 18 radial cracks were unique to either the Borofloat or Starphire layer. By scanning through both sides of the panel, the depth locations of these cracks were resolved. For 740-2, the intricate damage pattern was well represented in the C-scan image and the scan through the back face indicated no penetration into the Starphire layer. For 741-1, the bulk adhesive patterns did not appear to change as much as in the surface/near-surface images. The damage at the point of impact and crack in the corner were clearly visible, and small indications of damage were detected in the back face scan. With the XCT images for 741-2 indicating damage to the Starphire layer, the impact region and resulting radial cracks were as apparent through the strike face images as they were through the back face images. Overall, the C-scan images were very effective at representing the damage to each panel after air gun and sphere impact testing.

6. Quantitative Damage Threshold Results

A supplemental technique was developed for quantitatively estimating the percent damage in transparent laminate targets subjected to low velocity impact testing. Ultrasound C-scan imaging was chosen as the basis for obtaining a representative map to contrast damaged and undamaged regions through the bulk of the panels. This method was applied to C-scan images in which the bottom surface signal amplitude was mapped to represent volumetric damage through the bulk of each target. Each C-scan damage map was processed using an inverted grayscale in which the color "white" represented the highest degree of damage. Histograms of the selected C-scan damage maps were plotted as a function of grayscale levels on the *x*-axis and number of occurrences (or image pixels) on the *y*-axis. On each histogram, the *x*-axis ranged from black on the left side to white on the right side. Typically, there was a large curve or series of curves representing the undamaged region of the target. The damaged region was often represented by

a small curve at the right side of the histogram where the “white” or very light colors were present. A threshold was chosen on the histogram in which any occurrences to the right represented the damaged regions of the target and any occurrences to the left represented the undamaged regions. The idea was to separate and distinguish the total number of occurrences that represented undamaged and damaged regions of the C-scan image. This was often the most difficult step in the process, since a definitive threshold value was not always clear. Once the threshold value was determined, the histogram data containing the grayscale levels and number of occurrences was referenced. The grayscale level associated with the threshold was located and all occurrences to the right of this value (very light and “white” colors) were selected. The summation of total number of occurrences representing the damaged regions was calculated and this value was divided by the total number of all occurrences in the image and multiplied by 100 to acquire the estimated percent damage in the selected panel.

Estimated percent damage values were calculated for C-scan images representing the strike face and back face of each of the four transparent panels. The inverted grayscale images and corresponding histograms are shown in figure 5. For panels 740-1 and 741-2, which showed cone cracking in the Starphire layer and significant damage through the back face, the estimated percent damage increased. The damage increased from 10.9% to 15.7% for panel 740-1 due to the higher number of radial cracks present in the Starphire layer. For panel 740-2, in which there was no damage to the Starphire layer, the percent decreased from 8.7% to 0.0% since no damage could be detected in the C-scan image through the back face. For panel 741-1, the percent damage decreased from 1.8% to 1.5%. Despite the absence of a cone crack in the Starphire layer, the crack in the corner of the sample propagated through both the Eagle glass and Starphire layers, which accounted for the majority of damage through both the strike face and back face images. The quantitative damage threshold technique proved to be a useful means for estimating and comparing volumetric percent damage values for the transparent panels.

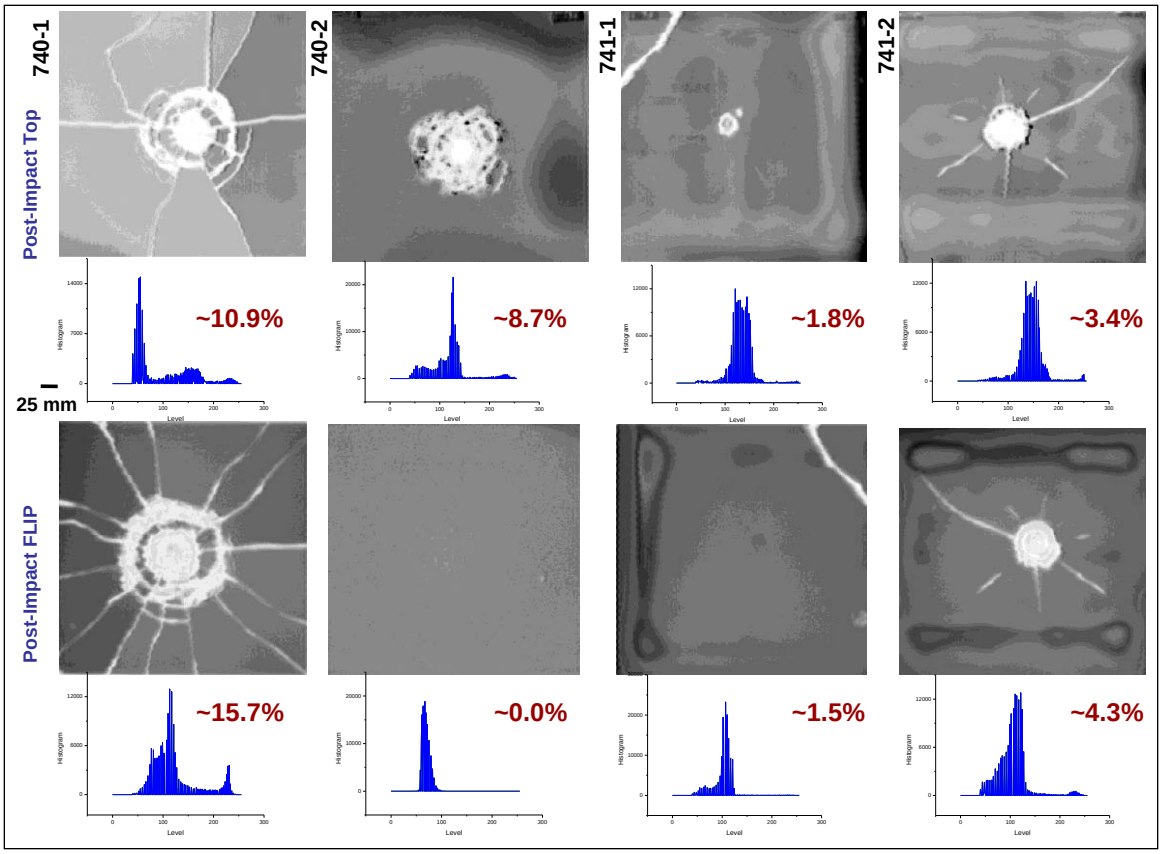

Figure 5. Quantitative histogram images and percent damage from the strike face and back face.

7. Multiple Impact Cumulative Damage Assessment

Cumulative damage in a single panel was evaluated by subjecting panel 740-2 to multiple impacts at the same location. The visual and nondestructive evaluation (NDE) damage results for 740-2 have been presented up to this point for a single impact. These results showed that the damage was contained within the Borofloat strike face layer and that no additional damage to the Starphire layer could be detected. The damaged panel was prepared for sphere impact under the same velocity conditions as the first test to induce a succession of three additional impacts to the same location where the first impact occurred. Visual inspection, cross-polarization imaging, and ultrasound C-scan imaging were conducted before and after each impact to study cumulative damage effects, as shown in figures 6 and 7.

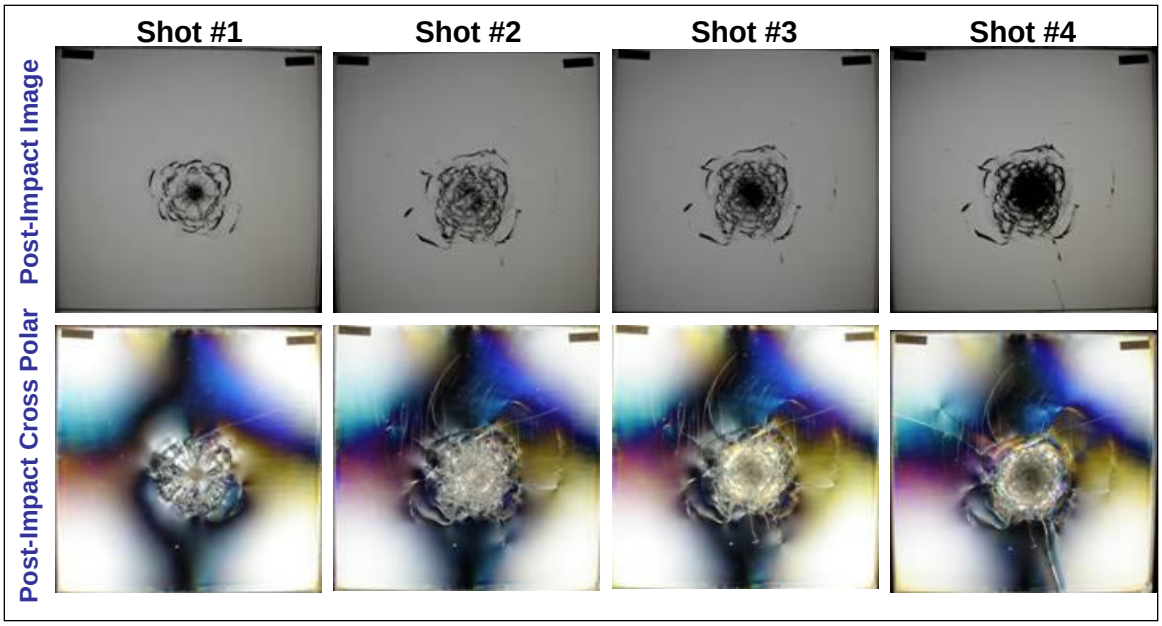

Figure 6. Visual and cross-polarized digital images of 740-2 after each of the four sphere impacts.

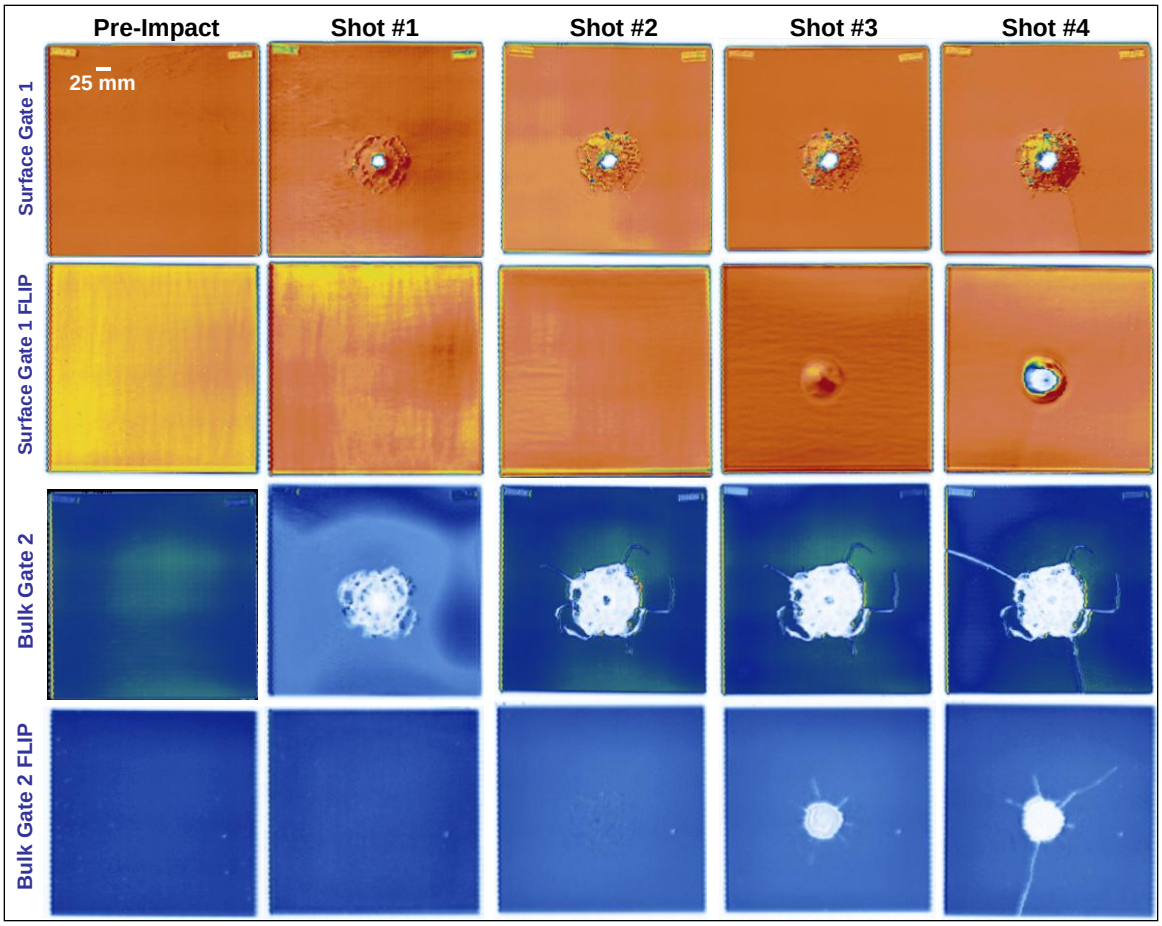

Figure 7. Surface and bulk C-scan images of 740-2 cumulative damage from the strike and back face.

Figure 6 shows the progression of damage through digital and cross-polarization images. After the second impact, multiple cracks formed within the original damage zone from the first impact. Several larger cracks also started to propagate, expanding the diameter of the damage zone. The damage to panel 740-2, as observed in the visual and cross-polarized images, did not appear to change significantly after the third impact. After the fourth and final impact, three of the cracks that had started to propagate after the second impact had fully propagated to the edge of the panel.

In figure 7, C-scan images of the surface/near surface of panel 740-2 after each impact are shown in succession, with the first row representing the strike face images and the second row representing the back face images. The strike face images showed the degree of damage at the point of impact and its slight degree of expansion after each impact. Damage due to cracking was not present until after the final impact, where a radial crack propagated to the lower edge of the panel. The back face images showed no indication of damage to the Starphire layer until after the third impact, at which point there appeared to be a slight physical deformation to the back face opposite the point of impact. After the fourth impact, a severe degree of damage resulting in complete signal loss was evident in the surface/near surface C-scan image. The third and fourth rows represented bulk C-scan images through the entire volume of panel 740-2. For the third row containing the strike face images, the damage zone expanded after the second impact, was very similar after the second and third impacts, and resulted in propagation of two radial cracks to the edge of the panel after the fourth impact. For the fourth row containing the back face images, some micro-cracking was evident after the second impact. The third impact revealed the presence of damage and the early formation of radial cracks within the Starphire layer. After the fourth impact, several of these radial cracks began to propagate, with one extending out to the edge of the panel. This demonstrated that out of the three edge cracks that were detected, one of them was present in the Starphire layer. These results showed a large contrast between panel 740-1, which had a large number of radial edge cracks after a single impact, and panel 740-2, in which four impacts to the same location were required to produce a radial edge crack.

The quantitative damage threshold technique was used to determine the increase in damage to the strike face and back face C-scan images after each of the four impacts, as shown in figure 8.

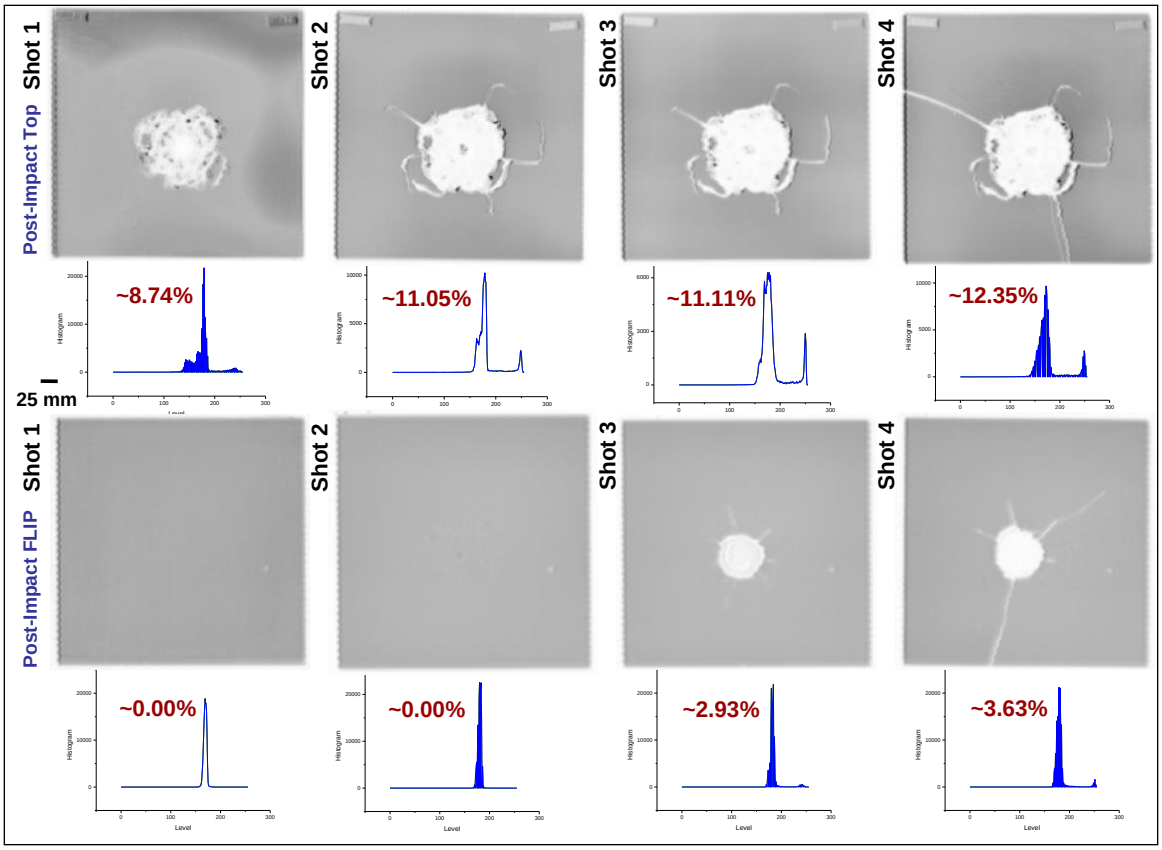

Figure 8. Histogram images and percent damage from the strike and back face of 740-2 after each impact.

For the strike face images, the quantitative results were consistent with the qualitative observations from visual inspection. The percent damage increased from 8.74% to 11.05% after the second impact with additional cracking to the damage zone and initial crack propagation, from 11.05% to 11.11% after the third impact with a minimal increase in damage, and from 11.11% to 12.35% after the fourth impact with radial crack propagation to the edges. For the back face images, there was no detectable damage after the first or second impacts, as the initial micro-cracking was not distinguished. After the third impact, the damage increased to 2.93% and again to 3.63% as one of the radial cracks propagated to the edge of the panel. All of the quantitative results consistently showed an increase in cumulative damage after each impact test.

8. Air/Tin Strike Face Comparison

An additional set of transparent laminate panels was fabricated to study the effect of conventional glass strike face type on low velocity impact. The Borofloat glass was fabricated in such a way that one side contained a residual layer of tin. The tin residue on the top of the glass was due to condensation of evaporated tin present in the atmosphere of the float bath (*12*). With two distinguishable surfaces (air-side up/tin-side up), it was important to determine which side

served as a better strike face. Two sets of panels were fabricated, one with the air-side up and one with the tin-side up. The tin-side-up panels, denoted 0310-T1 and 0310-T2, were identical in structure to 740-1 and 740-2. The air-side-up panels were denoted as 0310-A1 and 0310-A2. Air gun testing with ~19-mm steel sphere projectiles was used for all four panels. For 0310-A1, four tests were conducted with impacts of 6.7, 6.7, 7.2, and 13.0 m/s. For 0310-T1, three tests were conducted with impacts of 6.7, 6.7, and 15.0 m/s. For 0310-A2 and 0310-T2, a single impact with average velocity of ~24.6 m/s was used for each panel.

The same characterization methods used to evaluate the 740- and 741-series panels were applied to these panels. Visual characterization was conducted on the four panels in a pre-impact and post-impact state. Cross-polarization techniques were used to observe residual stress states before and after low velocity impact. The post-impact images are shown in figure 9. The four impacts to 0310-A1 and three impacts to 0310-T1 occurred at a high enough velocity to produce damage to the surface as well as delaminations in the two laminates. Despite multiple impacts to each panel, there did not appear to be any overlap between damage regions.

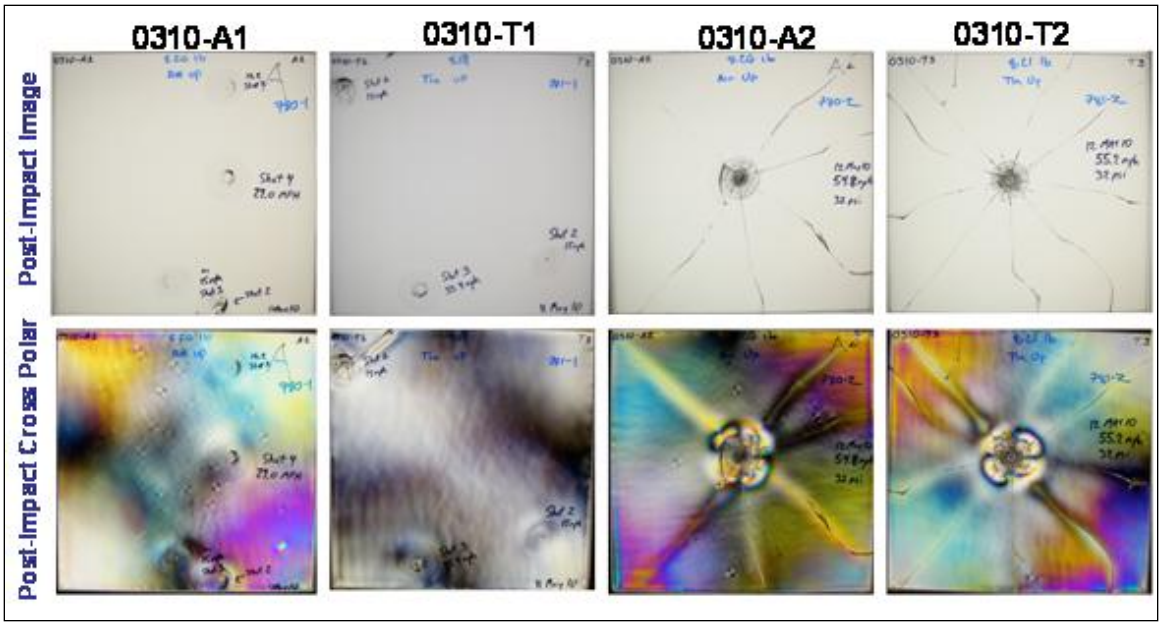

Figure 9. Visual characterization and cross-polarized images of the 0310-series post-impact.

In the cross-polarization images, panel 0310-T1 showed minor residual stress patterns while the other three panels displayed regions of higher residual stress, especially in the corner locations. The impacts to 0310-A2 and 0310-T2 both showed radial cracks originating from the point of impact and extending to the edge of each panel. In terms of the number of radial cracks, 0310-A2 exhibited 6 cracks as compared to 10 for 0310-T2, resulting in an improvement from the standpoint of visibility.

Ultrasound C-scan images were collected for all of the panels in both the pre- and post-impact states. Surface/near-surface images were mapped to show changes in signal amplitude at and near the point of impact of the Borofloat strike face. Bottom surface images were mapped to show changes in signal amplitude through the bulk of each panel. The post-impact surface/near surface images through the strike face and back face (rows 1 and 2, respectively) and post-impact bulk images through the strike face and back face (rows 3 and 4, respectively) are shown in figure 10. The surface/near-surface images for 0310-A1 and 0310-T1 were similar, with point of impact damage represented by complete loss of signal at each impact. The two highest velocity impact strikes resulted in the largest indications of residual surface damage. The surface/near-surface image for 0310-A2 exhibited a smaller degree of damage at the point of impact when compared to 0310-T2, but also showed a near-surface indication of a cone crack that connected two of the radial cracks. The images through the back face showed no detectable damage for 0310-A1 and 0310-T1, but both 0310-A2 and 0310-T2 showed surface indications of deformations resulting from a cone crack, as were previously detected in 740-1 and 741-2. The circular region representative of the bulge in the polycarbonate backing layer appeared to be larger in diameter for 0310-A2 as compared to 0310-T2.

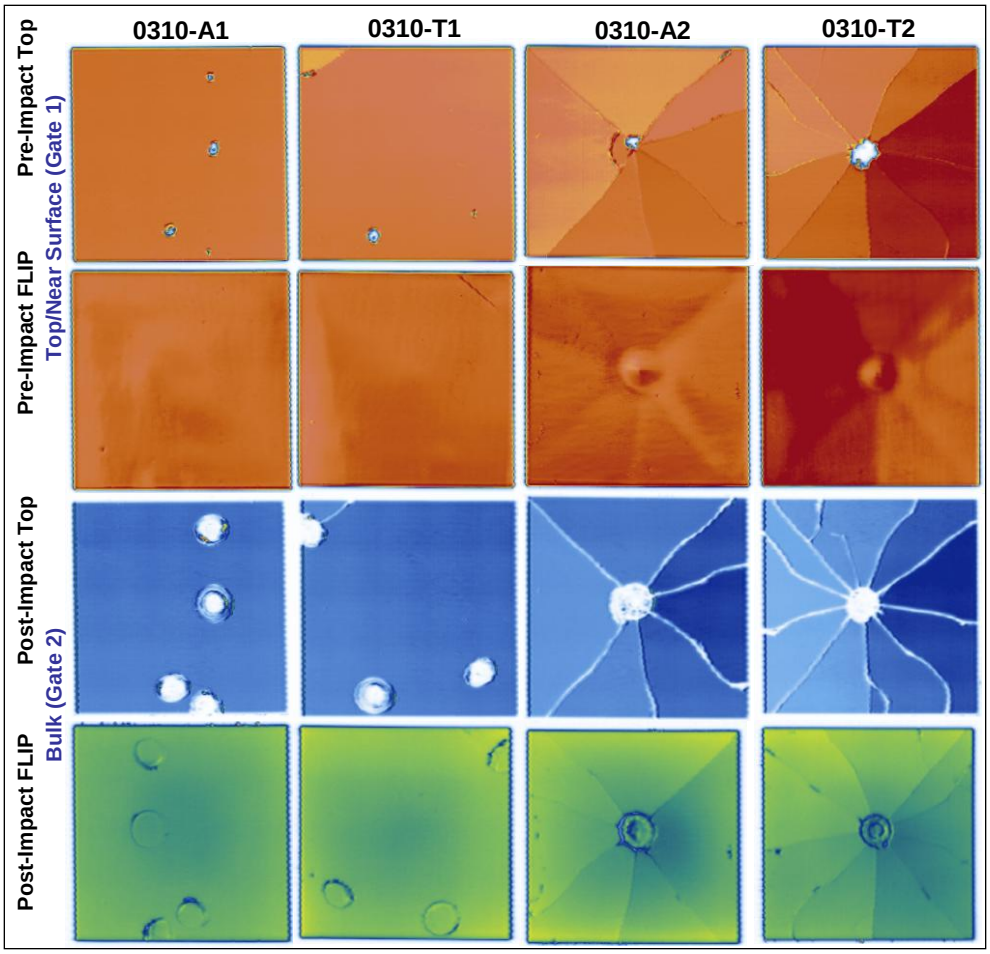

Figure 10. Surface/near-surface and bulk UT C-scan images of the 0310-series post-impact.

The bulk images for 0310-A1 and 0310-A2 revealed damage that was much larger in diameter than the surface/near-surface images. This indicated that the damage through the bulk of these panels was the result of delaminations at the Borofloat/Starphire interface. While the surface indications were much smaller, the diameter of damage due to delamination of the glass layers appeared to be similar regardless of the impact velocity. The C-scan images through the back face mirrored these results, highlighting the damage perimeter for each impact. The bulk images for 0310-A2 and 0310-T2 identified all of the cracks that were detected visually, clearly showing a partial crack and a crack that split off of one of the main radial cracks, each which was difficult to see in the digital and cross-polarization images. The bulk images through the back face also revealed small features near the edges of the panels that could not be resolved through visual means. The combination of surface/near-surface C-scan images through the strike and back faces provided a wealth of damage information that could not be otherwise detected.

The quantitative damage threshold technique was applied to determine the degree of damage through both the strike face and back face of all the 0310-series panels (figure 11). A direct comparison of panel 0310-A1, which had a total damage percent of 3.30%, and 0310-T1, which had a total damage percent of 2.14%, did not tell the whole story. Since 0310-A1 was subject to an additional impact and both panels were subject to impacts that demonstrated only half the damage since they occurred at the edges, the average damage per impact was a more useful value. While 0310-A1 had an average of 0.94% per impact, 0310-T1 was slightly lower at 0.85% per impact. For panel 0310-A2, which had a total damage percent of 3.21%, and 0310-T2, which had a total damage percent of 2.66%, the results appeared to be counterintuitive at first due to the difference in the number of cracks. However, while panel 0310-T2 exhibited 10 radial cracks, the percent damage appeared to be influenced more by the larger cone crack in 0310-A2, as evidenced in both the surface/near-surface and bulk images captured through the back face. The tin-side-up panel, 0310-T2, showed a higher number of radial cracks and the air-side-up panel, 0310-A2, indicated a larger cone crack, but the small variations in percent damage were not enough to definitively claim that one was superior to the other.

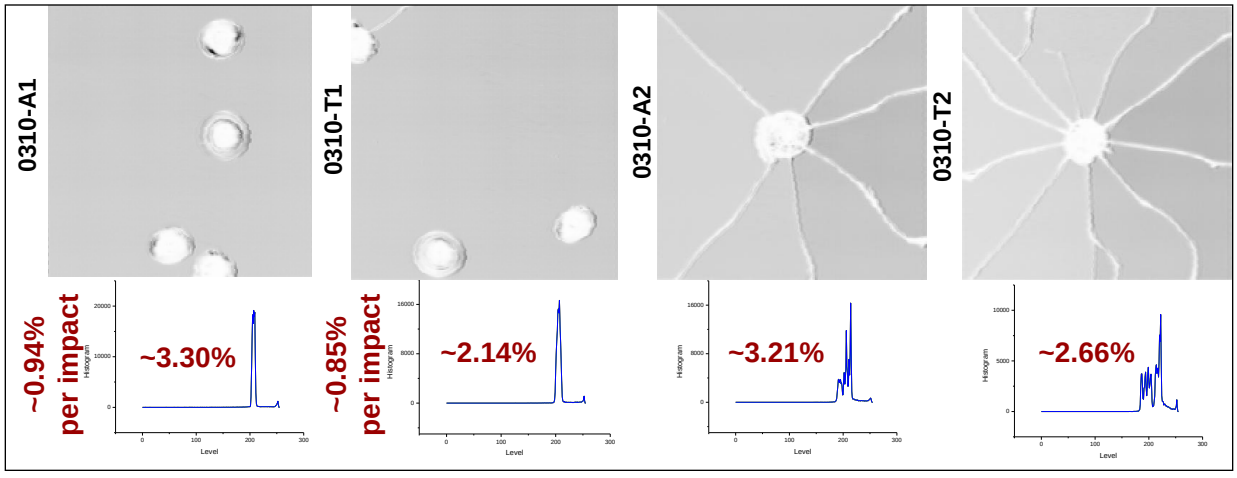

Figure 11. Histograms and percent damage from the strike faces of the 0310-series after impact.

9. Conclusions

Visual observation methods were shown to be effective for addressing visibility, one of the critical factors for evaluating transparent material performance. The simple qualitative tests of looking through the panel post-impact to observe damage or optical distortion, or quantitative tests of measuring the diameter of the impact region, were useful for comparing the utility of one laminate system to another. This method indicated that the 741-series transparent laminate system was the preferred choice due to the reduced average damage diameter. The 740-series panels showed extensive radial cracking that resulted in significant optical distortion. For obtaining a spatial map of stress in these multi-layer stacked laminate systems, cross-polarized imaging was instrumental for checking the integrity of each panel. Post-impact images were useful for determining whether stress was released or enhanced at or near the point of impact. While 740-2 showed the highest degree of pre-impact stress, it also revealed post-impact stress relief. Stress release at the strike face during cracking may have been the reason why there was no penetration into the Starphire layer.

While DR was not an effective characterization technique for mapping pre-impact defects or post-impact damage, XCT cross-sectional imaging was vital for evaluating damage as a function of depth. Not only did the XCT images reveal accurate damage dimensions, but also indicated whether or not the damage extended beyond the strike face. For two of the panels, cone cracks were found in the second glass layer that resulted in additional damage to the overall laminate system. XCT images were more effective than visual and cross-polarization imaging at determining which layer was damaged.

Ultrasound C-scan imaging also held several advantages. One was the ability to image changes in the adhesive layers that could not be physically seen. Ultrasound was also capable of detecting inclusions, scratches, and other surface and internal defects that were difficult or impossible to see visually. Dimensional changes to the polycarbonate backing layer were detected through C-scan imaging of the back face, another indication of damage beyond the strike face. For 740-1, in which there were significant differences in the radial crack patterns between the Borofloat strike face layer and the Starphire layer, C-scan imaging through different sides of the panel successfully mapped the distinct crack patterns in each layer. In addition to single impact results, cumulative damage was successfully studied by impacting panel 740-2 three additional times under the same conditions. As opposed to panel 740-1, which was subject to Starphire layer damage after a single impact, the Starphire layer in panel 740-2 remained undamaged until after the third strike. Due to the effectiveness of C-scan imaging for damage detection, a novel quantitative histogram technique was developed to calculate the estimated

percent damage based on these images. The results provided an effective means of comparing single impact damage from both sides of the panels as well as cumulative damage from multiple impacts.

These methods were also applied to conduct a comparison of conventional laminate panels in which the Borofloat layer was positioned with either a tin-side-up (standard) or air-side-up configuration. While damage characteristics were different in terms of the number of radial cracks and size of internal cone cracks, the quantitative histogram technique only revealed small differences in the percent damage under similar low velocity impact conditions, giving neither the clear advantage.

Overall, a combination of C-scan imaging and XCT cross-sectional imaging in addition to quantitative damage assessment from the histogram method provided a complete picture of transparent panel damage for various systems.

10. References

1. Patel, P. J.; Gilde, G. A.; Dehmer, P. G.; McCauley, J. W. Transparent Armor. *AMPTIAC Newsletter* **2000**, *4* (3).
2. Schott Borofloat glass. http://www.us.schott.com/borofloat/english/ (accessed May 2011).
3. PPG Starphire glass, Precision Glass and Optics data. http://www.pgo.com/pdf/ppg_starphire.pdf (accessed May 2011).
4. Corning Eagle glass. http://www.corning.com/displaytechnologies/en/products/eaglexg/index.aspx (accessed May 2011).
5. Feingold, J. M. Stress Diagnose It Before It Ruins Your Parts. *Plastics Technology* **2009**.
6. Hoffman, B. R. How to Measure Stress in Transparent Plastics. *Plastics Technology* **1998**.
7. Spring, K. R.; Parry-Hill, M. J.; Davidson, M. W. Michel-Levy Birefringence Chart. *Olympus Microscopy Resource Center* **2010**.
8. Stanley, J. H. Physical and Mathematical Basis of CT Imaging: ASTM Tutorial Section 3. *ASTM CT Standardization Committee* **1986**.
9. Newton, T. H.; Potts, D. G. Technical Aspects of Computed Tomography. *The C.V. Mosby Company* **1981**, *5*.
10. Mix, P. E. *Introduction to Nondestructive Testing*; John Wiley & Sons, 1987.
11. Krautkramer, J.; Krautkramer, H. *Ultrasonic Testing of Materials*; Springer-Verlag, 1990.
12. Muller, A. M.; Green, D. J. Elastic Indentation Response of Float Glass Surfaces. *Journal of the American Ceramic Society* **2010**, *93*, (1).

1 (PDF only) DEFENSE TECHNICAL INFORMATION CTR
DTIC OCA
8725 JOHN J KINGMAN RD
STE 0944
FORT BELVOIR VA 22060-6218

1 DIRECTOR
US ARMY RESEARCH LAB
IMNE ALC HRR
2800 POWDER MILL RD
ADELPHI MD 20783-1197

1 DIRECTOR
US ARMY RESEARCH LAB
RDRL CIO LL
2800 POWDER MILL RD
ADELPHI MD 20783-1197

1 DIRECTOR
US ARMY RESEARCH LAB
RDRL CIO MT
2800 POWDER MILL RD
ADELPHI MD 20783-1197

1 COMMANDER
US ARMY TACOM
PM SURVIVABLE SYSTEMS
SFAE GCSS W GSI H
M RYZYI
6501 ELEVEN MILE RD
WARREN MI 48397-5000

2 COMMANDER
US ARMY AMCOM
AVIATION APPLIED TECH DIR
J SCHUCK
FT EUSTIS VA 23604-5577

1 RUTGERS THE STATE UNIV
OF NEW JERSEY
DEPT OF CERAMIC & MTRL ENGR
R HABER
607 TAYLOR RD
PISCATAWAY NJ 0885

ABERDEEN PROVING GROUND

47 DIR USARL
RDRL SL
R COATES
RDRL WM
S KARNA
J MCCAULEY
RDRL WML
J NEWILL
RDRL WMM
J BEATTY
R DOWDING
P SMITH
RDRL WMM A
M MAHER
J SANDS
D SPAGNUOLO
RDRL WMM B
C FOUNTZOULAS
P MOY
J YU
RDRL WMM C
C PERGANTIS
RDRL WMM D
R BRENNAN (4 CPS)
R CARTER
E CHIN
K CHO
W GREEN (2 CPS)
R HOWELL
M PEPI
W ROY
R SQUILLACIOTI
D STRAND
S WALSH
W ZIEGLER
RDRL WMM E
M BRATCHER
J CAMPBELL
P DEHMER
G GILDE
J LASALVIA
P PATEL
T TAYLOR
RDRL WMM F
J ADAMS
K DOHERTY
E KLIER
RDRL WMP
P BAKER
RDRL WMP A
B RINGERS
RDRL WMP B
C HOPPEL
RDRL WMP C
T BJERKE
RDRL WMP E
M BURKINS
D HACKBARTH
RDRL WMP G
N ELDREDGE